ROV localization based on umbilical angle measurement

Christophe Viel, Juliette Drupt, Claire Dune, Vincent Hugel

ROV localization based on umbilical angle measurement

Christophe Viel*, Juliette Drupt**, Claire Dune***, Vincent Hugel***

* *CNRS, Lab-STICC, F-29806, Brest, France (e-mail: name.surname@gadz.org).*

** *Laboratoire Cosmer, Université de Toulon, France (e-mail: name.surname@gmail.com).*

*** *Laboratoire Cosmer, Université de Toulon, France (e-mail: name.surname@univ-tln.fr).*

ARTICLE INFO

Keywords:
Underwater robotics, cables model, localization system

ABSTRACT

If the umbilical of Remote Operated Vehicle (ROV) allows the transmission of information in real time or the supply of energy to the robot, it also has many disadvantages such as entanglement or the difficulty of predicting its shape, which raises the question of being able to do without it. In order to turn these constraints into advantages, this paper proposes a method to estimate the position of an ROV by observing the shape of its umbilical. The umbilical is equipped with moving ballasts and buoys to give it a predictable shape with straight lines: simple mathematical models of the umbilical can thus be defined. Using these models and measuring the angles at the ends of the cable, the position of the ROV can be found. Three umbilical models with different equipment are proposed. The methods were tested in a pool and the estimated position of the ROV was compared with its actual position measured using a motion capture system.

1. Introduction

Remotely Operated Vehicles (ROV) are underwater robots created to explore the seas where humans cannot do so directly. Their use and technology have developed rapidly over the past decades. However, to perform tasks such as exploration, map reconstruction or docking, a tracking system is required. The problem of underwater positioning is complex because GPS radio signals do not penetrate the water. An underwater equivalent could be the Underwater Wireless Sensor Networks (UWSNs), which have received a lot of attention in the last decade [2, 27]. UWSNs contain several components such as vehicles and sensors that are deployed in a specific acoustic area to perform collaborative monitoring and data collection tasks. These networks are used interactively between different nodes and ground-based stations, and can therefore be used for vehicle localization. In [25, 24] for example, an infrastructure-based localization scheme is proposed using four anchor nodes to form an UWSN, each located at known positions and broadcasting electromagnetic waves (EMW) at their own frequency. The localization of an Unmanned underwater vehicle (UUV) is performed using EMW and received signal strength (RSSs) to estimate distances and angles to the anchor nodes. However, UWSNs face many problems such as limited bandwidth, high propagation delay, power constraints, cost and installation of structures.

The most common solution for locating an underwater robot such as an ROV is Ultra Short Base Line (USBL). USBL is an underwater acoustic positioning method that consists of a transceiver under a vessel and a transponder on the vehicle. USBL calculates both a distance and an angle between the transceiver and the subsea beacon. However, USBL provides the position at a low update rate and sometimes with a lack of accuracy, so it is often combined with several sensors such as an inertial measurement unit (IMU), a camera, a barometer, or a sonar [1, 11, 23].

ORCID(s):

In the absence of USBL, sonars are a common solution for locating ROVs. In [32], the authors present a 3D mapping and localization (SLAM) approach for an underwater robot using only a depth sensor and a single-beam scanning sonar. Sonars can also be deported: [18] describes a method to detect and track a small ROV manipulator in successive sonar images taken by a main AUV. A convolutional neural network is applied to locate the agent in the sonar images.

Vision methods are also used underwater. [16, 17] describe the development of a position tracking system designed for an ROV using information provided by the vehicle camera and the projection of two laser pointers into the camera's optical field. [29] presents a vision-based location system for ROVs/AUVs. Underwater lights are used as light markers attached to the Tether Management System (TMS) cage to estimate and correct the ROV position. However, while vision methods can show good performance comparable to USBL, this performance is highly dependent on water turbidity and underwater visibility.

This works aims at defining a localization system dedicated to ROVs. The specificity of ROVs lies in their underwater umbilicals, allowing to transmit information in real time in both directions (see [5, 26]), to supply the robot with energy, and to maintain a lifeline with the robot to avoid losing it [22]. However, umbilicals present several problems, such as collision with external objects, entanglement, inertia and drag forces impacting navigation, cable breakage, etc... making it a trade-off between its constraints and its advantages [6]. Here the objective is to turn the disadvantage of the umbilical into an advantage by converting it into a localization system using a model of the umbilical and observing its shape.

To provide feedback on its position and shape, the umbilical can be modeled, equipped or instrumented. Two main categories of methods exist: detection of the umbilical, us-

ing vision [19, 20, 21] and/or sensors placed directly on/in the umbilical [7, 8, 12], and direct modeling of the umbilical using only the positions of the vessel and the ROV [13, 14, 10]. The main advantage of the first category is that an accurate model can be obtained in real time, but the equipment is often expensive and complex to install. In contrast, modeling strategies are cheap, but often less accurate and cannot always provide real-time results.

Several mathematical model exist to represent the shape and dynamics of the cable, from the simplest geometrical model such as the catenary curve [28] or the chain of segments [13], to the finite-element methods [10]. Geometrical models can simulate a large number of segments in real-time and are memory efficient, but with limited physical accuracy. In contrast, the Lumped-mass-spring method [4, 14, 15], which models the cable as mass points connected by massless elastic elements, and the segmental methods [9, 10, 3], which describe the cable as a continuous system and numerically solve the resulting partial differential equations, obtain accurate results but require a significant amount of computational time.

To provide a fast time computational model of the cable, the main author [31, 30] has proposed to equip the umbilical with ballasts or buoys moving freely on the cable, allowing it to be stretched and given a predictable shape. The umbilical can therefore be assimilated to predictable straight lines, simple to model and compute in real time. In the continuity of this work, this paper proposes a method to estimate the position of an ROV by observing the shape of its umbilical. By measuring the angles at the end of the cable and the depth of the ROV, the shape of the umbilical can be reconstructed using the straight line models, allowing the position of the ROV to be determined. Neither motorization nor TMS are used, which makes the method simple to implement. The experiments compare the result of the proposed method with the measurement of the umbilical shape by a motion capture system.

The main contributions of this works are

- a method to estimate the ROV position without USBL, UWSN or sonar,
- a proper umbilical model to be computed in real time by measuring only the angles at the ends of the cable and the depth of the ROV,
- a method that can be added easily to existing ROVs with a practical setup without motorization nor TMS.

The purpose of this research study and the assumptions are outlined in Section 2. Section 3 describes a localization method using a single sliding element to stretch the umbilical. Section 4 extends the method to two elements to stretch the umbilical. The results of experiments with both methods are compared with measured data in Section 5. Discussion and perspective are exposed in Section 6. Section 7 concludes this work.

2. Problematic and assumptions

Let $\mathcal{R}$ be the referential of origin $O = (0, 0, 0)$ corresponding to the coordinates of the boat where the first extremity of the umbilical is attached. $R = (x, y, z)$ are the coordinates of the ROV, corresponding to the second extremity of the umbilical. The vertical axis is oriented downwards, so for two (z_1, z_2), $z_1 > z_2$ means z_1 is deeper than z_2 and $z = 0$ corresponds to the sea surface.

In the absence of tension, a cable will take on an irregular shape. To prevent the cable from moving freely and becoming entangled with itself or its environment, a technique mostly used for shallow dives is to hang a ballast at a fixed length on the umbilical to stretch it between the boat and the ballast. When the ROV is close to the ballast, the cable between them takes the shape of a bell, similar to a catenary curve. However, the cable becomes like a straight line as the ROV moves away from the ballast due to the tension exerted by the ROV and the ballast. Since straight lines are easier to model, we propose to equip the umbilical with others elements such as buoys to keep the entire umbilical taut regardless the position of the ROV, similarly to [31].

A ballast or a buoy tied to a cable, namely "fixed", can usually only stretch one part of it, both in particular configuration. However, a ballast/buoy moving freely along the cable, namely "sliding", will always find its position at the lowest/highest point, corresponding to its minimum potential energy, where it stretches both parts of the cable simultaneously. Thus, a combination of fixed and sliding ballasts and/or buoys on the umbilical is an interesting solution to stretch it, and therefore to prevent cable entanglement. Once the umbilical is stretched, its shape becomes similar to straight lines, whose model can be determined analytically and used to reconstruct the shape of the umbilical. The ROV position can be found by measuring the angles at the ends of the cable.

The following assumptions are considered:

A1) The ratio of mass to buoyancy of the umbilical is negligible compared to the ballasts' weight and the buoys' buoyancy used in the configuration.

A2) The length variation of the umbilical is negligible compared to its length, considered constant.

A3) When the umbilical is taut, its geometry can be assimilated to straight lines between defined points, here the ballasts, the buoys, the boat and the ROV.

A4) The vertical position z of the ROV is known, and measured using a depth sensor for example.

A5) The boat and anchor are assumed to be strong/heavy enough to be unaffected by the action of the umbilical and ROV, and so can be considered motionless.

The study is divided into two parts: the first with a single sliding element, and the second with a fixed ballast and a sliding element. When necessary, some assumptions on the angles to be measured will be added.

3. Single element model

This section describes a method of localization with a single sliding element: a ballast or a buoy, as illustrated in Figure 1. The use a sliding ballast allows exploration near the surface, such as inspecting ship's hull, navigation under uniform ice, etc..., but is not suitable for seafloor exploration because the ballast must not touch it to keep the cable taut. Conversely, the use of a sliding buoy allows exploration near to the seafloor and not the surface.

3.1. System description

The parameters are illustrated in Figure 1. The umbilical of length l is divided in three parts: the first part $l_0 = \|OA\|$ between the boat O and an anchor A, the second part $l_1 = \|AB\|$ between the anchor A and a sliding element B (a ballast or buoy), and the last part $l_2 = \|BR\|$ between the sliding element B and the ROV R.

The cable $L = \|AR\|$ between the anchor and the ROV such that $L = l_1 + l_2$ has a fixed length. The sliding element can move freely on the cable L. Note that $l = l_0 + L$ and that l_0 can be taken equal to zero, *i.e.* the anchor A and the boat O are the same elements, *i.e.* $A = O$.

The oriented angles α and β are respectively the angle between the anchor A and the sliding element B, and between B and the ROV R in the plane $(O, \vec{x}, \vec{z})$. In the same way, let μ and η be the angles between the anchor A and the sliding element B, and between B and the ROV R in the plane $(O, \vec{y}, \vec{z})$.

Let l_{1x}, l_{1y}, l_{2x}, l_{2y} be the projections of l_1 and l_2 on the plane $(O, \vec{x}, \vec{z})$ and $(O, \vec{y}, \vec{z})$. The parameter s_b is defined such that $s_b = 1$ if the sliding element is a ballast, $s_b = -1$ if the sliding element is a buoy.

As shown in [31], the described configuration allows the umbilical to remain stretched in any quasi-static equilibrium and in presence of current and wave due to the the sliding element. In [31], the position (x, y, z) and forces applied on the sliding elements are supposed to be known, allowing to find the umbilical shape. Here, the objective is reverse: to find the coordinates of the ROV using the shape of the umbilical. As some parameters are unknown, the observed properties and hypotheses taken in [31] will not be exploited here. However, the following assumption is added:

A6) Angles α, β, μ and η can be measured.

Proposals for securing Assumption A6 in practice will be discussed in Section 6.

Parameters constraints

Let z_{floor} be the minimum depth, *i.e.* the seafloor or a rock, and h_B the height of the ballast or the height of the submerged part of the buoy. If the sliding element is a buoy, the anchor is the lowest element and so one must have $l_0 \leq z_{\text{floor}}$ to keep the umbilical stretched between the boat and the anchor. If the sliding element is a ballast, one must have $l_0 \leq z_{\text{floor}}$ and 1) either $l_0 + L \leq z_{\text{floor}}$ to allow the ROV to move without the ballast touching the seafloor in all cases, 2) or the ROV must maintain its depth such that the ballast does not touch the seafloor, *i.e.* $z < z_{\text{lim}}(x)$ where $z_{\text{lim}}(x) = 2\left(z_{\text{floor}} - h_M\right) - L\sqrt{1 - \left(\frac{x}{L}\right)^2}$ as described in [31, Section 4.1]. In the same way, the buoy must not touch the surface. However, since (x, z) are supposed to be initially unknown here, $z_{\text{lim}}(x)$ cannot be used and the worst case scenario with $(x, z) = (0, 0)$ is considered, leading to the following conditions

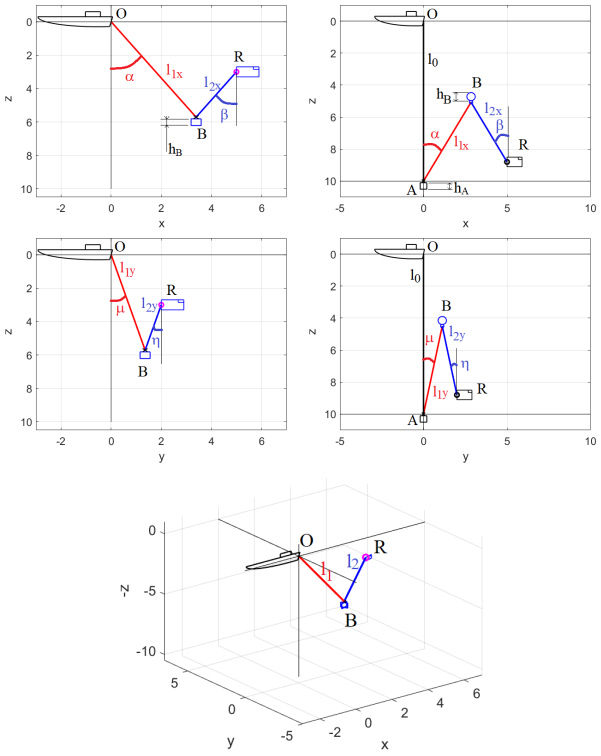

Figure 1: Parameters for a sliding ballast or buoy for (x, y, z)=(5, 2, 3), $L = 10$ and $l_0 = 0$ in the ballast case, and (x, y, z)=(5, 2, 8.8), $L = 10$ and $l_0 = L$ in the buoy case. R: ROV. B: sliding ballast or buoy. The black, red and blue lines correspond to l_0, l_1, l_2 . l_{1x}, l_{1y}, l_{2x}, l_{2y} are the projections of l_1 and l_2 on the plane $(O, \vec{x}, \vec{z})$ and $(O, \vec{y}, \vec{z})$.

$$L + l_0 + h_A \leq z_{\text{floor}} - h_B \quad \text{if } s_b = 1 \tag{1}$$

$$\begin{cases} l_0 + h_A & \leq z_{\text{floor}} \\ L & \leq l_0 - h_B \end{cases} \quad \text{if } s_b = -1. \tag{2}$$

where h_A is the height of the anchor.

3.2. Geometrical system

In a configuration where the umbilical is taut, the system can be expressed as

$$\begin{cases} x = & l_{1x}\sin(\alpha) + l_{2x}\sin(\beta) \\ y = & l_{1y}\sin(\mu) + l_{2y}\sin(\eta) \end{cases} \tag{3}$$

and

$$\begin{cases} z = & l_0 + s_b l_{1x}\cos(\alpha) - s_b l_{2x}\cos(\beta) \\ z = & l_0 + s_b l_{1y}\cos(\mu) - s_b l_{2y}\cos(\eta) \end{cases} \tag{4}$$

The relations between these projections can be expressed as

$$l_1^2 = l_{1x}^2 + \sin(\mu)^2\, l_{1y}^2 \tag{5}$$
$$l_2^2 = l_{2x}^2 + \sin(\eta)^2\, l_{2y}^2 \tag{6}$$
$$L = l_1 + l_2. \tag{7}$$

Using the steps described in Appendix A.1, one gets

$$l_{1x}^2 = \frac{l_1^2}{\left(1 + \tan(\mu)^2 \cos(\alpha)^2\right)} \tag{8}$$
$$l_{1y}^2 = \frac{l_1^2}{\left(\sin(\mu)^2 + \left(\frac{\cos(\mu)}{\cos(\alpha)}\right)^2\right)} \tag{9}$$

$$l_{2x}^2 = \frac{l_2^2}{\left(1 + \tan(\eta)^2 \cos(\beta)^2\right)} \tag{10}$$
$$l_{2y}^2 = \frac{l_2^2}{\left(\sin(\eta)^2 + \left(\frac{\cos(\eta)}{\cos(\beta)}\right)^2\right)}. \tag{11}$$

3.3. Calculation of the position (x, y, z)

From Assumptions A4 and A6, the depth z and the angles α, β, μ and η are known. Then, following the steps described in Appendix A.2, the length $l_1$and l_2 can be expressed as

$$l_1 = L - l_2 \tag{12}$$
$$l_2 = \frac{\left(\frac{L\cos(\alpha)}{a_1} - s_b\left(z - l_0\right)\right)}{\left(\frac{\cos(\alpha)}{a_1} + \frac{\cos(\beta)}{a_2}\right)} \tag{13}$$

where

$$a_1 = \sqrt{1 + \tan(\mu)^2 \cos(\alpha)^2} \tag{14}$$
$$a_2 = \sqrt{1 + \tan(\eta)^2 \cos(\beta)^2}. \tag{15}$$

The length l_1 and l_2 can so be obtained if z, α, β, μ and η are known. Thus, using (12)-(13) and the measured parameters, l_{1x}, l_{1y}, l_{2x} and l_{2y} can be evaluated using (8)-(11). Then, the position (x, y) can be obtained using (3).

4. Two-element model

This section presents a method of localization with two elements: a ballast fixed to the umbilical at a constant distance from the boat, and a sliding element, ballast or buoy, that can move freely between the ballast and the ROV, inspired from [31]. Compared to the strategy proposed in Section 3, the ROV can operate close to the seafloor and in a large area using the full length of the umbilical l. The ballast compensates for some of the action of the buoy, inducing less effort for the ROV. However, its movements remain limited when it is close to the surface.

4.1. System description

Parameters are illustrated in Figure 2. Consider here the configuration with a sliding element described in Section 3 but where the anchor 1) is not strong enough to compensate for the actions of the current and umbilical, 2) or has been replaced by a ballast that is too light to be considered as an anchor. In both cases, let us call the fixed element "ballast M" in the rest of the study and keep the notation B for the sliding element, buoy or ballast. The umbilical is still divided in three parts $l_0 = \|OM\|$, $l_1 = \|MB\|$ and $l_2 = \|BR\|$, where M is put at a fixed distance $l_0 > 0$.

Let's defined the oriented angles γ and ϕ between the boat O and the ballast M in the plane $\left(O, \vec{x}, \vec{z}\right)$ and $\left(O, \vec{y}, \vec{z}\right)$. Note that this configuration becomes equivalent to the one in Section 3 when the ballast is perfectly vertical, *i.e.* when $\gamma = 0$ and $\phi = 0$. Let l_{0x}, l_{0y} be the projection of l_0 on the plane $\left(O, \vec{x}, \vec{z}\right)$ and $\left(O, \vec{y}, \vec{z}\right)$.

The main advantage of this configuration is that it allows to explore a larger area using the length l_0. To ensure that l_0 stays stretched, a condition is that the ballast M must be taken stronger than the buoy B, as shown in [31, Assumption A8]. Again, the described configuration allows the umbilical to stay stretched in all quasi-static equilibrium.

A7) In addition to α, β, μ and η, considered that γ and ϕ can be measured.

In the following sections, the study will be illustrated using a sliding buoy, *i.e.* $s_b = -1$, but the same study can be performed with a sliding ballast.

Parameters constraints

Let define h_M the height of the ballast which has replaced the anchor. By taking h_M instead of h_A, the same constraints on l_0 and L described in Section 3.1 must be taken into account, following the same logic. Moreover, the ballast M is fixed on the umbilical and is not motionless like the anchor A in Section 3. Thus, an additional condition must be taken to keep the umbilical taut. A minimum depth $z_{\min}$ is defined such that the ROV must always dive to a depth less than $z_{\min}$, *i.e.* $z > z_{\min}$. Otherwise, the cable l_0 is not tensioned because the ROV is too close to the surface for the ballast M to stretch l_0 and L simultaneously. As shown in [31, Section 5], $z_{\min}$ can be expressed as

$$z_{\min}(x) = \begin{cases} \sqrt{l_0^2 - x^2} - L + h_B & \text{if } \left(|x| < \sqrt{l_0^2 - L^2}\right) \,\&\, \left(l_0 > L\right), \\ \sqrt{L^2 - x^2} - l_0 + h_B & \text{if } \left(|x| < \sqrt{L^2 - l_0^2}\right) \,\&\, \left(L > l_0\right), \\ h_B & \text{else.} \end{cases} \tag{16}$$

However, since (x, z) are supposed to be initially unknown here, the worst case scenario with $(x, z) = (0, 0)$ can be considered, leading to take $z_{\min}(0)$ in all situations. Note that if the parameters are chosen such that $l_0 = L$, $z_{\min}(x)$ does not exist.

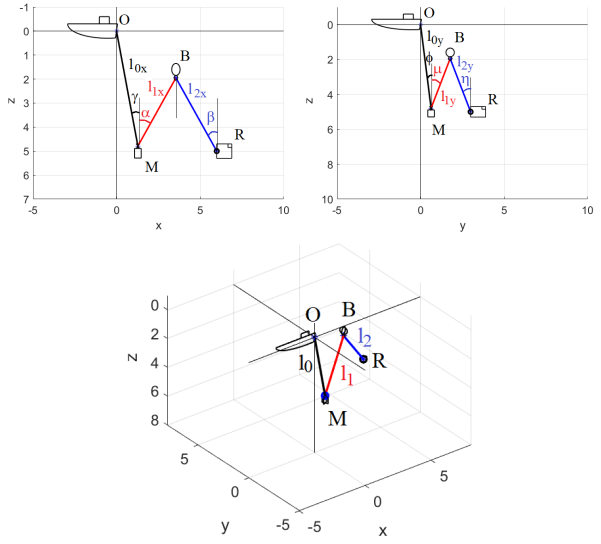

Figure 2: Parameters for the ballast and the sliding buoy for (x, y, z)=$(6, 5, 3)$, $L = 8$, $l_0 = 5$. R: ROV. B: sliding ballast or buoy. The black, red and blue lines correspond to l_0, l_1, l_2. l_{0x}, l_{0y}, l_{1x}, l_{1y}, l_{2x}, l_{2y} are the projections of l_0, l_1 and l_2 on the plane $(O, \vec{x}, \vec{z})$ and $(O, \vec{y}, \vec{z})$. An other configuration can be obtained by exchanging the buoy B with a sliding ballast.

4.2. Geometrical system

In a configuration where the umbilical is taut, the system can be expressed as

$$\begin{cases} x = l_{0x}\sin(\gamma) + \quad l_{1x}\sin(\alpha) + l_{2x}\sin(\beta) \\ y = l_{0y}\sin(\phi) + \quad l_{1y}\sin(\mu) + l_{2y}\sin(\eta) \end{cases} \tag{17}$$

and

$$\begin{cases} z = \quad l_{0x}\cos(\gamma) + s_b l_{1x}\cos(\alpha) - s_b l_{2x}\cos(\beta) \\ z = \quad l_{0y}\cos(\phi) + s_b l_{1y}\cos(\mu) - s_b l_{2y}\cos(\eta) \end{cases} \tag{18}$$

Note that (17)-(18) is equal to (3)-(4) if $\gamma = 0$ and $\phi = 0$, which is the case if the ballast M is heavy enough to be considered as an anchor.

As shown in Appendix B.1, the relations between l_{1x}, l_{1y} and l_{2x}, l_{2y} can still be expressed with (5)-(11). Since the length of l_0 is fixed, the relation between l_{0x}, l_{0y} and l_0 can be expressed as

$$l_0^2 = l_{0x}^2 + \sin(\gamma)^2 l_{0y}^2. \tag{19}$$

Using steps described in Appendix B.1, one gets

$$l_{0x}^2 = \frac{l_0^2}{\left(1 + \tan(\phi)^2\cos(\gamma)^2\right)} \tag{20}$$

$$l_{0y}^2 = \frac{l_0^2}{\left(\sin(\phi)^2 + \left(\frac{\cos(\phi)}{\cos(\gamma)}\right)^2\right)}. \tag{21}$$

It is to be noted that since l_0 is known and constant, l_{0x} and l_{0y} can be evaluated if γ and ϕ are known.

4.3. Calculation of the position (x, y, z)

From Assumptions A4, A6 and A7, the depth z and the angles γ, ϕ, α, β, μ and η are known. Then, following the steps described in Appendix A.2, the length l_1 and l_2 can be expressed as

$$l_1 = L - l_2 \tag{22}$$

$$l_2 = \frac{\frac{L\cos(\alpha)}{a_1} - s_b\left(z - l_0\cos(\gamma)\right)}{\frac{\cos(\alpha)}{a_1} + \frac{\cos(\beta)}{a_2}} \tag{23}$$

where

$$a_1 = \sqrt{1 + \tan(\mu)^2\cos(\alpha)^2} \tag{24}$$

$$a_2 = \sqrt{1 + \tan(\eta)^2\cos(\beta)^2}. \tag{25}$$

Note that if $\gamma = 0$, *i.e.* the ballast M is an anchor that allows l_0 to remain vertical, (22)-(23) become equal to (12)-(13).

The length l_1 and l_2 can so be obtained if z, α, β, γ, μ and η are known, and so l_{1x}, l_{1y}, l_{2x} and l_{2y} using (8)-(11). Moreover, l_{0x} and l_{0y} can be evaluated if γ and ϕ are known using (20)-(21). Then, the position (x, y) can be obtained using (17).

5. Experimental test

5.1. Material description

The configurations described in Sections 3 and 4 were tested in the pool of the Cephismer, Base Navale of Toulon, France. The umbilical was equipped with reflective markers at 20cm intervals so that its position could be tracked using the Qualisys [1] motion capture system. The displacement of each umbilical point was measured with the ROV in motion and processed using the software Qualisys Track Manager.

The force exerted by a buoy is evaluated in grams, corresponding to the maximum mass it can lift. Three configurations illustrated in Figure 3 were tested with the following parameters:

- 1 sliding ballast B of mass 240g, $l_0 = 0$m and $L = 2.6$m, see Figure 3a.
- 1 sliding buoy B of mass 130g and an anchor A of 2kg, $l_0 = 2.75$m and $L = 3$m, see Figure 3b.
- 1 fixed ballast M of mass 240g and 1 siding buoy B of mass 130g, $l_0 = 2.2$m and $L = 2.2$m, see Figure 3c.

The sliding elements were obtained using a neutrally buoyant pulley shown in Figure 3d. The size of the pool is 7.2m× 4.2m with a depth of 3m.

Let (x_i, y_i, z_i) be the coordinate of the i-th position measured and $(\hat{x}_i, \hat{y}_i)$ the estimation of (x_i, y_i) obtained using the measured angles, (22)-(23) and (17), with $\gamma = 0$ and $\phi = 0$ for the cases with a single element. Note that $\hat{z}_i = z_i$ because z_i is supposed to be measured.

[1] https://www.qualisys.com

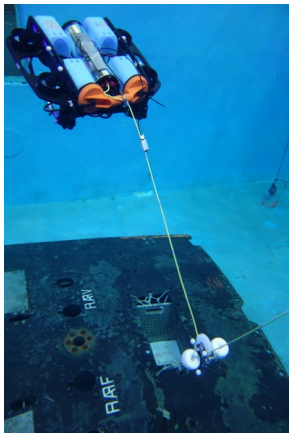

(a) Sliding ballast

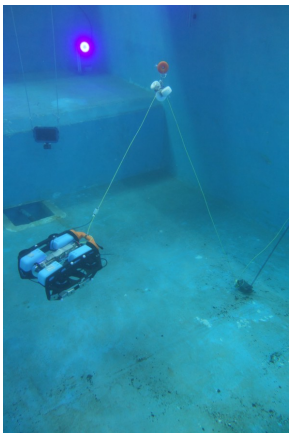

(b) Sliding buoy and anchor

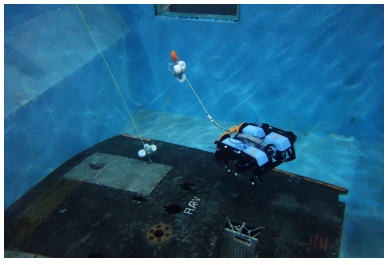

(c) Fixed ballast and sliding buoy.

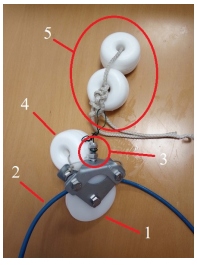

(d) Pulley for sliding buoy

Figure 3: Configurations tested in the pool of the Cephismer. d: Pulley for sliding buoy. 1: pulley. 2: umbilical. 3: ball joint to reduce twist effort between buoy and pulley. 4: additional buoy and ballast to give neutral buoyancy to the pulley assembly. 5: buoys for the self-management strategy.

For the number N of points measured by the motion capture, the average position error E_d relative to the method is

$$E_d = \sum_{i=1}^{N} \sqrt{\left(x_i - \hat{x}_i\right)^2 + \left(y_i - \hat{y}_i\right)^2}. \tag{26}$$

5.2. Angles measurement

Let L_a be the list of measured angles $L_a = \{\alpha, \beta, \gamma, \mu, \eta, \phi\}$. Here, the angles were estimated with the motion capture system using the coordinate of two points measured on the umbilical. In the absence of this motion capture system, L_a could be measured by equipping the umbilical with sensors, for example IMUs, see Section 6.

Let M^* be, depending on the chosen configuration, the boat O is if $l_0 = 0$, the anchor A if $l_0 \neq 0$ and A is heavy enough to respect Assumption A5, the ballast M otherwise. Let also $P_0 \in OM$, $P_1 \in M^*B$ and $P_2 \in BR$ be three points measured on the umbilical, illustrated in Figures 4 and 6. For $I \in \{P_0, P_1, P_2, O, M, M^*, B, R\}$, let (x_I, y_I, z_I) be the coordinates of point I. The angles L_a can be evaluated using

$$\alpha = \operatorname{atan}\left(\frac{|x_{P1} - x_{M^*}|}{|z_{P1} - z_{M^*}|}\right) \tag{27}$$

$$\mu = \operatorname{atan}\left(\frac{|y_{P1} - y_{M^*}|}{|z_{P1} - z_{M^*}|}\right) \tag{28}$$

$$\beta = \operatorname{atan}\left(\frac{|x_R - x_{P2}|}{|z_R - z_{P2}|}\right) \tag{29}$$

$$\eta = \operatorname{atan}\left(\frac{|y_R - y_{P2}|}{|z_R - z_{P2}|}\right) \tag{30}$$

$$\gamma = \operatorname{atan}\left(\frac{|x_{P0} - x_M|}{|z_{P0} - z_M|}\right) \tag{31}$$

$$\phi = \operatorname{atan}\left(\frac{|y_{P0} - y_M|}{|z_{P0} - z_M|}\right) \tag{32}$$

An ideal measurement would be to take $P_0 = O$ and $P_1 = P_2 = B$ to evaluate L_a. However, for several reasons such as the fact that B is sliding, these points may be difficult or impossible to measure in practice without a motion capture system. Thus, the proposed method was evaluated by taking points such that a sensor could be installed at these positions. These "sensors" positions have to be chosen such that

1. they must avoid blocking the movement of the sliding element on the umbilical as much as possible,
2. they are far enough to obtain a good estimate of the umbilical orientation,
3. the distance between the sensor and the axis of rotation of the angles it measures is realistic.

Two estimates of the angles are evaluated and compared in the next section:

- with ideal measurement taking $P_0 = O$ and $P_1 = P_2 = B$,
- where P_0, P_1 and P_2 simulate sensors position fixed on the umbilical, respecting the three conditions exposed above. Here, P_0, P_1 and P_2 were selected such that $\|P_0M\| = 110$cm, $\|M^*P_1\| = 40$cm, $\|P_2R\| = 20$cm, as illustrated in red in Figures 4 and 6.

5.3. Results

Figures 4 and 5 show the results obtained with a single element. Considering the non-ideal measurement, an average error $E_d = 0.043$m was measured with the ballast and $E_d = 0.107$m with the buoy. Figure 6 shows the results obtained with two elements, and a measurement of $E_d = 0.108$m. These figures show that the discrepancy between the theoretical and current positions is small, even while the ROV is moving. The umbilical remained perfectly taut during all tests. The position estimation appears to be more accurate with one element than two: it is surely due to the angle measurement error that accumulates with the

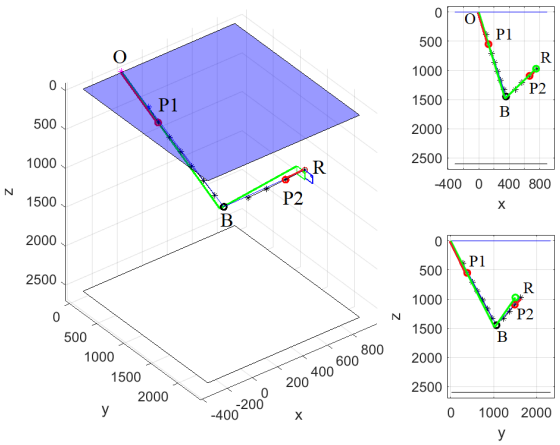

(a) With sliding mass

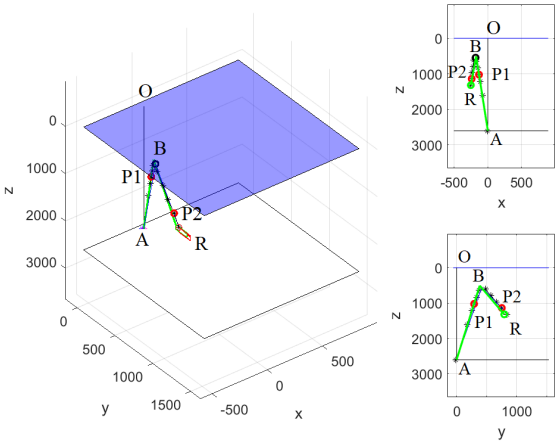

(b) With sliding buoy

Figure 4: Estimation of the ROV position with single sliding element. In black, measured umbilical positions. In green, estimated umbilical and ROV positions. Red dots and lines represent points used to estimate umbilical angles.

second method. Indeed, when the angles are evaluated using ideal measurements $P_0 = O$ and $P_1 = P_2 = B$, one gets an average error E_d below 0.38m in all cases (green curves): the comparison of the results showed that the accuracy of the method is directly proportional to the accuracy of the angle measurement. By keeping the same measurement point but with a longer cable, the cable will look less like a straight line and, therefore, the accuracy of the estimated position will likely decrease. However, the tests are very promising and experiments using sensors to directly measure the angles are planned for further developments.

6. Discussion and perspective

6.1. Perspective: angles measurement

In Section 5, angles were estimated using positions measured with a motion capture system. To implement this system in practice, we propose to install IMUs at several positions on the umbilical corresponding to the points P_0, P_1 and P_2 in Figures 4 and 6, *i.e.* two IMUs for the single element

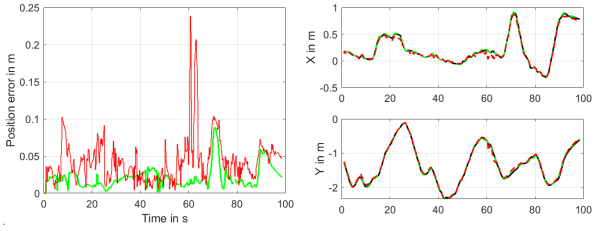

(a) Left: position error with sliding mass. Right: ROV trajectory. Green: $E_d = 0.021$m. Red: $E_d = 0.043$m.

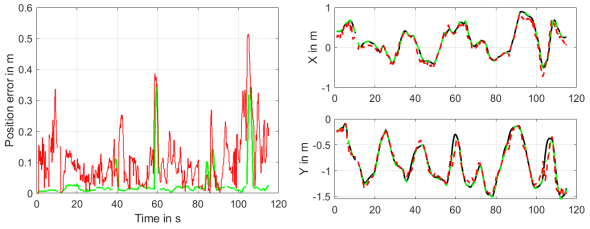

(b) Left: position error with sliding buoy. Right: ROV trajectory. Green: $E_d = 0.028$m. Red: $E_d = 0.107$m.

Figure 5: Position error with sliding mass or buoy. Holes in curve line correspond to missing data in the motion capture. Black line: current ROV position. Green lines: estimation made with ideal measurement. Red lines: estimation made with non-ideal measurement.

model and three for the two-element model.

The angles β and η can be easily obtained installing an IMU near R (see P_1) and connecting it directly to the ROV: the information can then be transmitted via the umbilical. The main inconvenient is that the sensor blocks the displacement of the sliding element between it and the ROV. Since an IMU placed far from the ROV provides a better estimate of the angle, its position is a compromise between element displacement and measurement accuracy.

The angles α and μ can also be easily obtained when $l_0 = 0$ by installing the IMU at the origin of the umbilical O and receiving the information on the boat. When $l_0 \neq 0$, the sensor must be installed far underwater, so a communication cable is needed to transmit the sensor data to the surface. Since there is no sliding element on l_0, this cable can be attached to l_0 without creating any inconvenience.

The angles γ and ϕ can be measured at the umbilical origin, or at the ballast M, as illustrated by P_0 in Figure 6. Since a cable is required to receive information for α and μ, the second option is preferred to group the two sensors at the same location, as in Section 5. In addition, placing the IMU in this position reduces the influence of the waves. Both sensors can use the same communication cable. Since there is no sliding elements on l_0, the sensor can be placed at a position P_0 at a larger distance from M than for P_1 to obtain an accurate angle measurement.

6.2. Discussion: Influence of dynamics and waves

The proposed method has a maximum accuracy when the umbilical is kept stretched by the ballast and buoy. Each time the ROV descends, ascends or retreats, a part of the um-

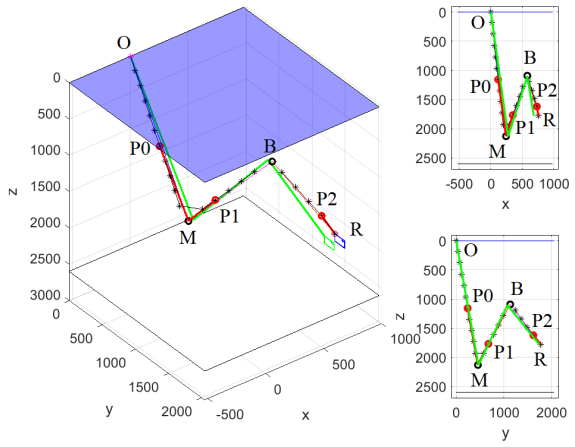

(a) Estimation of ROV position. In green, estimated umbilical and ROV position. Red dots and lines are points used to estimate umbilical angles.

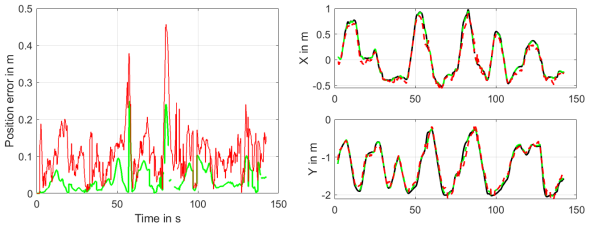

(b) Right: position error. Right: ROV trajectory. Black line: current ROV position. Dash red line: estimated ROV position. Green: $E_d = 0.038$m. Red: $E_d = 0.108$m.

Figure 6: Estimation of the ROV position with a fixed mass M and sliding buoy B. In black, measured umbilical positions. Holes in curve lines correspond to missing data in the motion capture sequence. Green lines: estimation made with ideal measurement. Red lines: estimation made with non-ideal measurement.

bilical becomes temporary loose. To keep the cable taut, the ballast and the buoy must be chosen so that their behavior is faster than the ROV's movement, *i.e.*, the ballast dives faster than the ROV descends and the buoy rises faster than the ROV ascends. To prevent a too heavy ballast or a too strong buoy from inducing a significant drag force on the umbilical, an alternative approach is to control the ROV to move slower than the rise of the buoy or the fall of the ballast. A similar method can be used to counteract the effect of waves: to ensure the umbilical stays stretched even in the presence of waves, the weight of the anchor or the ballast must allow it to accelerate and fall faster than the wave, which is the same for the rise of the buoy. Both methods are described in more detail in [31].

7. Conclusion

This paper presents a method to estimate the position of an ROV by observing the shape of its umbilical. By equipping the umbilical with moving ballast and/or buoy, the cable takes a predictable shape with straight lines, simple to model. By measuring the angles at the ends of the cable and the depth of the ROV, the shape of the umbilical can be reconstructed from these straight line models and therefore the position of the ROV can be determined. Three mathematical models of the umbilical with different equipment are proposed to find the position of the ROV. The sliding ballast and buoy also allow avoiding entanglement of the cable with itself or with the surrounding obstacles, without motorization or TMS, easy to set up. The method was tested in the pool with a motion capture system to measure the umbilical angles and obtain the current position of the ROV. A position error of 10cm for 3m of umbilical was measured, making this method interesting to study. However, the accuracy of the method is directly proportional to the accuracy of the angle measurement.

In future work, IMUs will be installed to obtain the angles at the ends of the umbilical, and thus show the validity of the method as a localization system.

References

[1] M. Audric. Gaps, a new concept for usbl [global acoustic positioning system for ultra short base line positioning]. In *Proc. IEEE Techno-Ocean'04*, volume 2, pages 786–788, 2004.

[2] K. Mahmood Awan, P. A. Shah, K. Iqbal, S. Gillani, W. Ahmad, and Y. Nam. Underwater wireless sensor networks: A review of recent issues and challenges. *Wireless Communications and Mobile Computing*, 1, 2019.

[3] O. Blintsov. Development of the mathematical modeling method for dynamics of the flexible tether as an element of the underwater complex. *Eastern-European Journal of Enterprise Technologies*, 1 (7):4–14, 2017.

[4] B. Buckham and M. Nahon. Dynamics simulation of low tension tethers. In *IEEE Conference Proceedings Oceans*, volume 2, pages 757–766, 1999.

[5] R. D. Christ and R. L. Wernli Sr. *The ROV manual: a user guide for observation class remotely operated vehicles*. Elsevier, 2011.

[6] T. Crandle, G. Cook, and E. Celkis. Tradeoffs between umbilical and battery power in rov performance. In *IEEE OCEANS 2017-Anchorage*, pages 1–6, 2017.

[7] J. Drupt, C. Dune, A. I. Comport, S. Seillier, and V. Hugel. Inertial-measurement-based catenary shape estimation of underwater cables for tethered robots. In *IROS (to appear)*, Kyoto, Japan, 2022. IEEE/RSJ.

[8] R. G. Duncan, Mark E. Froggatt, S. .T Kreger, R. J. Seeley, D. K. Gifford, A. K. Sang, and M. S. Wolfe. High-accuracy fiber-optic shape sensing. In *Sensor Systems and Networks*, volume 6530, page 65301S, 2007.

[9] O. A. Eidsvik and I. Schjølberg. Time domain modeling of rov umbilical using beam equations. *IFAC*, 49(23):452–457, 2016.

[10] O. A. N. Eidsvik and I. Schjølberg. Finite element cable-model for remotely operated vehicles (rovs) by application of beam theory. *Ocean Engineering*, 163:322–336, 2018.

[11] S. Fan, C. Liu, B. Li, Y. Xu, and W. Xu. Auv docking based on usbl navigation and vision guidance. *Journal of Marine Science and Technology*, 24(3):673–685, 2019.

[12] J. E. Frank, R. Geiger, D. R. Kraige, and A. Murali. Smart tether system for underwater navigation and cable shape measurement, 2013. US Patent 8,437,979, URL https://patents.google.com/patent/US8437979B2/en.

[13] O. Ganoni, R. Mukundan, and R. Green. Visually realistic graphical simulation of underwater cable. *Computer Science Research Notes*, 2018.

[14] F. González, A. de la Prada, A. Luaces, and M. González. Real-time simulation of cable pay-out and reel-in with towed fishing gears. *Ocean Engineering*, 131:295–307, 2017.

[15] Sung Min Hong, Kyoung Nam Ha, and Joon-Young Kim. Dynamics modeling and motion simulation of usv/uuv with linked underwater cable. *Journal of Marine Science and Engineering*, 8(5):318, 2020.

[16] G. C. Karras and K. J. Kyriakopoulos. Localization of an underwater vehicle using an imu and a laser-based vision system. In *Mediterranean Conference on Control & Automation*, pages 1–6, 2007.

[17] G. C. Karras, D. J. Panagou, and K. J. Kyriakopoulos. Target-referenced localization of an underwater vehicle using a laser-based vision system. In *OCEANS*, pages 1–6, 2006.

[18] J. Kim and S.-C. Yu. Convolutional neural network-based real-time rov detection using forward-looking sonar image. In *Proc IEEE/OES Autonomous Underwater Vehicles*, pages 396–400, 2016.

[19] M. Laranjeira, C. Dune, and V. Hugel. Catenary-based visual servoing for tethered robots. In *IEEE International Conference on Robotics and Automation*, pages 732–738, 2017.

[20] M. Laranjeira, C. Dune, and V. Hugel. Embedded visual detection and shape identification of underwater umbilical for vehicle positioning. In *OCEANS 2019-Marseille*, pages 1–9, 2019.

[21] M. Laranjeira, C. Dune, and V. Hugel. Catenary-based visual servoing for tether shape control between underwater vehicles. *Ocean Engineering*, 200:107018, 2020.

[22] A. Lasbouygues, S. Louis, B. Ropars, L. Rossi, H. Jourde, H. Délas, P. Balordi, R. Bouchard, M. Dighouth, M. Dugrenot, et al. Robotic mapping of a karst aquifer. In *IFAC: International Federation of Automatic Control*, 2017.

[23] F. Mandić, I. Rendulić, N. Mišković, and Đ. Nađ. Underwater object tracking using sonar and usbl measurements. *Journal of Sensors*, 1, 2016.

[24] D. Park, J. Jung, K. Kwak, W. K. Chung, and J. Kim. 3d underwater localization using em waves attenuation for uuv docking. In *Proc. IEEE Underwater Technology (UT)*, pages 1–4, 2017.

[25] D. Park, K. Kwak, J. Kim, and W. K. Chung. 3d underwater localization scheme using em wave attenuation with a depth sensor. In *Proc. IEEE ICRA*, pages 2631–2636, 2016.

[26] H. Stuart, S. Wang, O. Khatib, and M. R. Cutkosky. The ocean one hands: An adaptive design for robust marine manipulation. *The International Journal of Robotics Research*, 36(2):150–166, 2017.

[27] X. Su, I. Ullah, X. Liu, and D. Choi. A review of underwater localization techniques, algorithms, and challenges. *Journal of Sensors*, 1, 2020.

[28] M. Such, J. R. Jimenez-Octavio, A. Carnicero, and O. Lopez-Garcia. An approach based on the catenary equation to deal with static analysis of three dimensional cable structures. *Engineering structures*, 31(9):2162–2170, 2009.

[29] P. Trslić, A. Weir, J. Riordan, E. Omerdic, D. Toal, and G. Dooly. Vision-based localization system suited to resident underwater vehicles. *Sensors*, 20(2):529, 2020.

[30] C. Viel. Self-management of rov umbilical using sliding buoys and stop. *IEEE Robotics and Automation Letters*, 7(3):8061–8068, 2022.

[31] C. Viel. Self-management of the umbilical of a rov for underwater exploration. *Ocean Engineering*, 248:110695, 2022.

[32] J. Wang, S. Bai, and B. Englot. Underwater localization and 3d mapping of submerged structures with a single-beam scanning sonar. In *Proc. IEEE ICRA*, pages 4898–4905, 2017.

A. Proof for sliding element

A.1. Calculation of l_{1x}, l_{2x} and l_{1y}, l_{2y}

Let z_B be the coordinate of the ballast/buoy B on the axis $\vec{O}z$. Since z_B can be evaluated in the planes (O, x, z) and (O, y, z), one has

$$z_B = l_0 + s_b l_{1x} \cos(\alpha) = l_0 + s_b l_{1y} \cos(\mu) \tag{33}$$

$$z_B = z - s_b l_{2x} \cos(\beta) = z - s_b l_{2x} \cos(\eta) \tag{34}$$

Using (33)-(34), one gets

$$l_{1x} = l_{1y} \frac{\cos(\mu)}{\cos(\alpha)} \tag{35}$$

$$l_{2x} = l_{2y} \frac{\cos(\eta)}{\cos(\beta)}. \tag{36}$$

Using (5) and (35), one gets

$$\begin{aligned} l_1^2 &= l_{1x}^2 + \sin(\mu)^2 l_{1y}^2 \\ l_1^2 &= l_{1x}^2 + \sin(\mu)^2 \left(\frac{\cos(\alpha)}{\cos(\mu)}\right)^2 l_{1x}^2 \\ l_1^2 &= \left(1 + \tan(\mu)^2 \cos(\alpha)^2\right) l_{1x}^2 \\ l_{1x}^2 &= \frac{l_1^2}{\left(1 + \tan(\mu)^2 \cos(\alpha)^2\right)}. \end{aligned} \tag{37}$$

In the same way, one can obtain using again (5) and (35)

$$\begin{aligned} l_1^2 &= l_{1x}^2 + \sin(\mu)^2 l_{1y}^2 \\ l_1^2 &= l_{1y}^2 \left(\frac{\cos(\mu)}{\cos(\alpha)}\right)^2 + \sin(\mu)^2 l_{1y}^2 \\ l_{1y}^2 &= \frac{l_1^2}{\left(\sin(\mu)^2 + \left(\frac{\cos(\mu)}{\cos(\alpha)}\right)^2\right)}. \end{aligned} \tag{38}$$

The same calculation can be made for l_{2x}^2, l_{2z}^2 using respectively (36)-(6).

A.2. Calculation of l_1 and l_2

Considering (4)

$$\begin{aligned} z &= l_0 + s_b l_{1x} \cos(\alpha) - s_b l_{2x} \cos(\beta) \\ s_b\left(z - l_0\right) &= l_{1x} \cos(\alpha) - l_{2x} \cos(\beta) \end{aligned} \tag{39}$$

since $s_b \in \{-1, 1\}$. Introducing (8) and (10), one gets

$$\begin{aligned} s_b\left(z - l_0\right) =& \frac{l_1 \cos(\alpha)}{\sqrt{1 + \tan(\mu)^2 \cos(\alpha)^2}} \\ &- \frac{l_2 \cos(\beta)}{\sqrt{1 + \tan(\eta)^2 \cos(\beta)^2}}. \end{aligned} \tag{40}$$

Setting $a_1 = \sqrt{1 + \tan(\mu)^2 \cos(\alpha)^2}$ and $a_2 = \sqrt{1 + \tan(\eta)^2 \cos(\beta)^2}$. Since $L = l_1 + l_2$, (40) becomes

$$\begin{aligned} s_b\left(z - l_0\right) &= \frac{L \cos(\alpha)}{a_1} - l_2 \left(\frac{\cos(\alpha)}{a_1} + \frac{\cos(\beta)}{a_2}\right) \\ l_2 &= \frac{\frac{L\cos(\alpha)}{a_1} - s_b\left(z - l_0\right)}{\frac{\cos(\alpha)}{a_1} + \frac{\cos(\beta)}{a_2}} \end{aligned} \tag{41}$$

and so

$$l_1 = L - \frac{\frac{L\cos(\alpha)}{a_1} - s_b\left(z - l_0\right)}{\frac{\cos(\alpha)}{a_1} + \frac{\cos(\beta)}{a_2}}. \tag{42}$$

Lengths l_1 and l_2 can so be obtained if z, α, β, μ and η are known.

B. Proof for two elements

B.1. Calculation of l_{0x} and l_{0y}

Let z_M be the coordinate of the ballast M on the $\vec{O}z$ axis and z_B the coordinate of the buoy B on the $\vec{O}z$ axis. Since z_M and z_B can be evaluated in the plans (O, x, z) and (O, y, z), one has

$$z_M = l_{0x}\cos(\gamma) = l_{0y}\cos(\phi) \tag{43}$$

$$z_B = l_{0x}\cos(\gamma) - l_{1x}\cos(\alpha) = l_{0y}\cos(\phi) - l_{1y}\cos(\mu) \tag{44}$$

$$z_B = z - l_{2x}\cos(\beta) = z - l_{2x}\cos(\eta) \tag{45}$$

From (43)-(45), one gets

$$l_{0x} = l_{0y}\frac{\cos(\phi)}{\cos(\gamma)} \tag{46}$$

$$l_{1x} = l_{1y}\frac{\cos(\mu)}{\cos(\alpha)} \tag{47}$$

$$l_{2x} = l_{2y}\frac{\cos(\eta)}{\cos(\beta)}. \tag{48}$$

Note that (47)-(47) are identical to (35)-(36), so (5)-(11) are still valid.

Considering now l_0, using (19) and (46), one gets

$$\begin{aligned} l_0^2 &= l_{0x}^2 + \sin(\phi)^2 l_{0y}^2 \\ l_0^2 &= l_{1x}^2 + \sin(\phi)^2 \left(\frac{\cos(\gamma)}{\cos(\phi)}\right)^2 l_{0x}^2 \\ l_0^2 &= \left(1 + \tan(\phi)^2\cos(\gamma)^2\right) l_{0x}^2 \\ l_{0x}^2 &= \frac{l_0^2}{\left(1 + \tan(\phi)^2\cos(\gamma)^2\right)}. \end{aligned} \tag{49}$$

In the same way, one can obtain using again (19) and (46)

$$\begin{aligned} l_0^2 &= l_{0x}^2 + \sin(\phi)^2 l_{0y}^2 \\ l_0^2 &= l_{0y}^2 \left(\frac{\cos(\phi)}{\cos(\gamma)}\right)^2 + \sin(\phi)^2 l_{0y}^2 \\ l_{0y}^2 &= \frac{l_0^2}{\left(\sin(\phi)^2 + \left(\frac{\cos(\phi)}{\cos(\gamma)}\right)^2\right)}. \end{aligned} \tag{50}$$

B.2. Calculation of l_0, l_1 and l_2

Let's study (18). Since $s_b \in \{-1, 1\}$, one has

$$z = l_0\cos(\gamma) + s_b l_{1x}\cos(\alpha) - s_b l_{2x}\cos(\beta)$$

$$s_b\left(z - l_0\cos(\gamma)\right) = l_{1x}\cos(\alpha) - l_{2x}\cos(\beta). \tag{51}$$

Introducing (8) and (10) in 51, one gets

$$s_b\left(z - l_0\cos(\gamma)\right) = \frac{l_1\cos(\alpha)}{\sqrt{1 + \tan(\mu)^2\cos(\alpha)^2}} - \frac{l_2\cos(\beta)}{\sqrt{1 + \tan(\eta)^2\cos(\beta)^2}}. \tag{52}$$

Setting $a_1 = \sqrt{1 + \tan(\mu)^2\cos(\alpha)^2}$ and $a_2 = \sqrt{1 + \tan(\eta)^2\cos(\beta)^2}$. Since $L = l_1 + l_2$, (52) becomes

$$\begin{aligned} s_b\left(z - l_0\cos(\gamma)\right) &= \frac{L\cos(\alpha)}{a_1} - l_2\left(\frac{\cos(\alpha)}{a_1} + \frac{\cos(\beta)}{a_2}\right) \\ l_2 &= \frac{\frac{L\cos(\alpha)}{a_1} - s_b\left(z - l_0\cos(\gamma)\right)}{\frac{\cos(\alpha)}{a_1} + \frac{\cos(\beta)}{a_2}}. \end{aligned} \tag{53}$$

Using $L = l_1 + l_2$ again, one obtains also

$$l_1 = L - \frac{\frac{L\cos(\alpha)}{a_1} - s_b\left(z - l_0\cos(\gamma)\right)}{\frac{\cos(\alpha)}{a_1} + \frac{\cos(\beta)}{a_2}}. \tag{54}$$

Lengths l_1 and l_2 can so be obtained if z, α, β, γ μ and η are known. Note that if $\gamma = 0$, *i.e.* the ballast M is an anchor that allows l_0 to remain vertical, (54) becomes equal to (42).

Considering now l_{0x} and l_{0y}, since l_0 is known and constant, if γ and ϕ are known, l_{0x} and l_{0y} can be evaluated using (20) and (21).